The Algebraic Parametric Coupler Point Curve Equation

M. John D. Hayes[1] and Mirja Rotzoll[2]

[1] Department of Mechanical and Aerospace Engineering, Carleton University, Ottawa, ON, K1S 5B6, Canada,
john.hayes@carleton.ca,
WWW home page: https://carleton.ca/johnhayes/
[2] Canada Border Services Agency, Ottawa, ON, Canada

Abstract. There are six distinct input-output (IO) equations for any given four-bar 4R linkage that relate distinct pairs of the four exterior angles between the edges of the deformable quadrilateral. The algebraic v_i-v_j IO equation expresses one joint angle tangent half-angle parameter, v_i, in terms of another, v_j, as an implicit biquadratic function scaled by the link lengths. In this paper a novel method is presented using the v_1-v_2 IO equation for deriving the parametric coupler point curve equation for both assembly modes in terms of the input angle parameter v_1, expressed in the non-moving linkage reference coordinate system. To do this, the v_1-v_2 equation is solved for v_2 and the result is substituted into the forward kinematics 4×4 homogeneous transformation matrix for the open 2R kinematic chain of the first two moving links. Finally, the coupler point coordinates in the x_2, y_2 coordinate system that moves with the coupler are transformed into the relatively non-moving x_0, y_0 linkage coordinate system, yielding the parametric coupler point curve equation.

Keywords: v_1-v_2 equation, coupler point curve, computational geometry

1 Introduction

The mechanical problem of guiding a point along a planar curve using a four-bar linkage jointed with four revolute joints (generally referred to as a 4R mechanism) has been investigated extensively over the last 150 years since the first published results of Samuel Roberts in 1875 [1]. The trigonometric coupler point curve equation reported in that work is an implicit expression in terms of the lengths of the links and the coupler geometry. There is no direct way to map the location of a single point on the coupler curve generated by an arbitrary 4R mechanism to the corresponding configuration of the linkage, i.e., the joint angles required to reach that point, using the trigonometric equation. This presents a significant challenge for applications where force transmission quality of the mechanism must be considered as the coupler point traces the curve, as in pick-and-place operations for manufacture and assembly for example. Therefore, the

research objective of the present work is to determine a parametric form of the coupler point curve equation explicitly in terms of the joint angles. Since Study's kinematic mapping will be relied upon to determine the algebraic IO equations used to obtain the desired results, the mapping will be briefly summarised in what follows.

1.1 Study's Kinematic Mapping

The rigid body displacement group for two and three dimensional spaces are conveniently represented using 3×3 and 4×4 homogeneous transformations matrices derived using the Denavit and Hartenberg (DH) parameters [2, 3]. There are several possibilities to parameterise the matrix representation of this rigid body displacement group, one of them being the kinematic mapping that was originally formulated by Eduard Study and reported in an appendix of his book "Geometrie der Dynamen" [4] in 1903. It defines every distinct Euclidean displacement as a distinct point on a six-dimensional quadric hyper-surface, now known as the Study quadric S_6^2, in a seven-dimensional projective space, $\mathbb{P}^7$. A point on S_6^2 consists of eight homogeneous coordinates, not all zero, $[x_0 : x_1 : x_2 : x_3 : y_0 : y_1 : y_2 : y_3]$ which Study called a "soma", a Greek word meaning "body". The hyper-surface is a seven-dimensional bilinear quadratic equation given by

$$x_0y_0 + x_1y_1 + x_2y_2 + x_3y_3 = 0, \tag{1}$$

excluding the *exceptional generator*, which we call A_∞, where $x_0 = x_1 = x_2 = x_3 = 0$, having the parametric representation

$$[0 : 0 : 0 : 0 : y_0 : y_1 : y_2 : y_3].$$

A_∞ does not represent any real displacement, but it nonetheless plays an important role as a generator space.

For a soma to represent a real displacement in $SE(3)$, it must satisfy two conditions: the first being Equation (1); the second being the inequality

$$x_0^2 + x_1^2 + x_2^2 + x_3^2 \neq 0. \tag{2}$$

Equation (1) contains only bilinear cross terms. This implies that the quadric has been rotated out of its standard position, or normal form. It is straightforward to diagonalise the quadratic form of Equation (1) which reveals that this six-dimensional quadric in $\mathbb{P}^7$ has the normal form

$$x_0^2 + x_1^2 + x_2^2 + x_3^2 - y_0^2 - y_1^2 - y_2^2 - y_3^2 = 0, \tag{3}$$

which is analogous to the Plücker quadric, P_4^2, of line geometry. The normal form of S_6^2 shows that it is a six-dimensional hyperboloid of one sheet doubly-ruled by special 3-space generators in two opposite reguli, which we call A-planes and B-planes, after [5].

It can be shown that lines on S_6^2 represent either a one parameter set of translations or rotations. The lines which contain the 1×8 identity array [1 :

$0:0:\ldots:0]$, which Study called the "protosoma", are either the one parameter rotation or translation subgroups. The exceptional generator A_∞ is an A-plane. In general, two different A-planes do not intersect, nor do two different B-planes, but there are exceptions [6]. An A-plane corresponds to $SO(3)$ if it contains the identity and its intersection with A_∞ is the empty set, and to $SE(2)$ if it contains the identity and intersects A_∞ in a line. These two types of A-planes intersect each other in lines on S_6^2. Each of these lines represent rotations about the line orthogonal to the plane of the planar displacement and through the centre point of the spherical displacement [6, 7]. The only B-planes that intersect A_∞ correspond to the subgroup of all translations, while in general the intersection of an A-plane and a B-plane is either a point, or a two dimensional plane [8].

The Study soma coordinates, also known as Study parameters, are defined using the elements of the 4×4 homogeneous transformation matrix $\mathbf{T}$,

$$\mathbf{T} = \begin{bmatrix} 1 & \mathbf{0}_{1\times 3} \\ \mathbf{t}_{3\times 1} & \mathbf{A}_{3\times 3} \end{bmatrix} = \begin{bmatrix} 1 & 0 & 0 & 0 \\ t_{10} & a_{11} & a_{12} & a_{13} \\ t_{20} & a_{21} & a_{22} & a_{23} \\ t_{30} & a_{31} & a_{32} & a_{33} \end{bmatrix}.$$

The 3×3 rotation submatrix elements are denoted as $\mathbf{A} = (a_{ij})$ with $i, j \in \{1, 2, 3\}$ while the translation vector elements are denoted as $\mathbf{t} = (t_{k0})$ with $k \in \{1, 2, 3\}$. The homogeneous quadruple $x_0 : x_1 : x_2 : x_3$ can be obtained from at least one of the following ratios:

$$\begin{aligned} x_0 : x_1 : x_2 : x_3 &= 1 + a_{11} + a_{22} + a_{33} : a_{32} - a_{23} : a_{13} - a_{31} : a_{21} - a_{12}; \\ &= a_{32} - a_{23} : 1 + a_{11} - a_{22} - a_{33} : a_{12} + a_{21} : a_{31} + a_{13}; \\ &= a_{13} - a_{31} : a_{12} + a_{21} : 1 - a_{11} + a_{22} - a_{33} : a_{23} + a_{32}; \\ &= a_{21} - a_{12} : a_{31} + a_{13} : a_{23} + a_{32} : 1 - a_{11} - a_{22} + a_{33}. \end{aligned} \quad (4)$$

The remaining four coordinates $y_0 : y_1 : y_2 : y_3$ are linear combinations of the x_i and t_{k0} and are computed as

$$\begin{aligned} y_0 &= \tfrac{1}{2}(t_{10}x_1 + t_{20}x_2 + t_{30}x_3), \quad & y_1 &= \tfrac{1}{2}(-t_{10}x_0 + t_{30}x_2 - t_{20}x_3), \\ y_2 &= \tfrac{1}{2}(-t_{20}x_0 - t_{30}x_1 + t_{10}x_3), \quad & y_3 &= \tfrac{1}{2}(-t_{30}x_0 + t_{20}x_1 - t_{10}x_2). \end{aligned} \quad (5)$$

Study developed the method to compute the four x_i parameters directly from the 3×3 rotation submatrix $\mathbf{A}$ via one of the four sets of ratios expressed in Equation (4). In general each of the four yield the same ratios. But in certain instances, for example when $\mathbf{A}$ describes a rotation through angle π, one or more of the four ratios in Equation (4) result in $x_0 : x_1 : x_2 : x_3 = 0 : 0 : 0 : 0$, the exceptional generator. But for every rotation matrix $\mathbf{A}$ at least one of the four ratios does not result in four zeros. Study also showed that the mapping is bijective, meaning that for each point on S_6^2 there is one and only one Euclidean displacement represented by the homogeneous 4×4 transformation matrix $\mathbf{T}$:

$$\mathbf{T} = \frac{1}{\delta}\begin{bmatrix} x_0^2+x_1^2+x_2^2+x_3^2 & 0 & 0 & 0 \\ 2(-x_0y_1+x_1y_0-x_2y_3+x_3y_2) & x_0^2+x_1^2-x_2^2-x_3^2 & 2(-x_0x_3+x_1x_2) & 2(x_0x_2+x_1x_3) \\ 2(-x_0y_2+x_1y_3+x_2y_0-x_3y_1) & 2(x_0x_3+x_1x_2) & x_0^2-x_1^2+x_2^2-x_3^2 & 2(-x_0x_1+x_2x_3) \\ 2(-x_0y_3-x_1y_2+x_2y_1+x_3y_0) & 2(-x_0x_2+x_1x_3) & 2(x_0x_1+x_2x_3) & x_0^2-x_1^2-x_2^2+x_3^2 \end{bmatrix}$$

where $\delta = x_0^2 + x_1^2 + x_2^2 + x_3^2$. The first column is the associated translation of the Euclidean displacement and the elements of the lower right 3×3 submatrix are the nine a_{ij} of the associated rotation matrix $\mathbf{A}$.

1.2 Algebraic Input-Output Equations

Recently, the v_i-v_j algebraic input-output (IO) equations for planar [9], spherical [10], and spatial 4R mechanisms [11] have been introduced in the literature. Because a 4R four-bar mechanism is a planar, spherical, or spatial deformable quadrangle, there are six distinct pairs of joint angles between different pairs of edges. Consider the planar 4R mechanisms illustrated in Figures 1b and 1c. The six distinct angle pairings are θ_1-θ_2, θ_1-θ_3, θ_1-θ_4, θ_2-θ_3, θ_2-θ_4, and θ_3-θ_4.

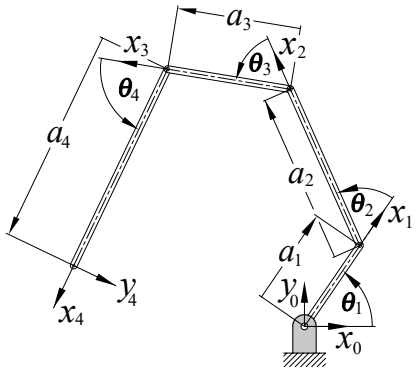

(a) Open 4R kinematic chain.

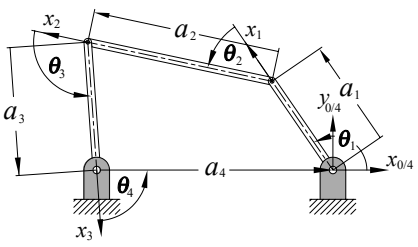

(b) Counter-clockwise closed 4R chain.

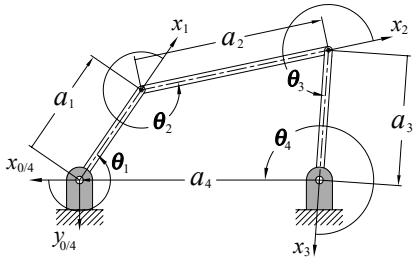

(c) Clockwise closed 4R chain.

Fig. 1: Counter-clockwise and clockwise joint angle circulation.

An algorithm that generalises the procedure for determining the algebraic IO equations for any four-bar linkage kinematic architecture, planar, spherical, and spatial, using only algebraic means can be found in the Ph.D. thesis of Mirja Rotzoll [12]. The linkage is initially considered as an open kinematic chain, and Figure 1a describes its kinematic geometry using the original Denavit-Hartenberg (DH) convention [2, 3]. The resulting forward kinematics transformation matrix for the open chain is then mapped into Study's kinematic mapping image space as the eight soma coordinates defined in [13] and expressed in Equations (4) and (5). This mapping allows one to characterise the displacement from the base to the end-effector frame as a set of eight linearly independent algebraic varieties in the seven-dimensional projective kinematic mapping image space. To obtain a simple closed kinematic chain that represents the mechanism, the open chain is conceptually closed by equating the obtained algebraic parametrisation to its identity, leading to a set of equations that completely describe the linkage kinematics. We have chosen to close the kinematic chain such that there is a counter-clockwise circulation of joints, see Figure 1b. However, clockwise joint circulation will yield identical results with the exception that joint angles will have different zeros, see Figure 1c. The clockwise joint axis circulation requires that the non-moving reference coordinate systems $x_{0/4}$, $y_{0/4}$ be rotated by π radians to be in accordance with the original DH convention [2, 3]. With the help of elimination theory, the given system of eight polynomial equations is manipulated leading to a single polynomial that depends on only two of the four joint variables. This is done for each of the six distinct pairs of joint variables leading to six algebraic IO equations for each four-bar linkage kinematic architecture.

The attention of this paper will be focused on the IO equation that relates the joint angles θ_1 and θ_2 to each other. But in the derivation, the tangent half-angle parameters for θ_1, θ_2, θ_3, and θ_4 are used, making the resulting equations algebraic. Let the input angle parameter be v_1 and the output angle parameter be v_4, where $v_i = \tan\theta_i/2$. In [12], two elimination steps were applied to the Gröbner bases of the ideal generated by the Study soma coordinates to eliminate the angle parameters v_2 and v_3 from the equations. This results in the algebraic IO equation relating the v_1 and v_4 angle parameters, which we call the v_1-v_4 IO equation:

$$Av_1^2v_4^2 + Bv_1^2 + Cv_4^2 - 8a_1a_3v_1v_4 + D = 0, \tag{6}$$

where

$$\begin{aligned}
A &= A_1A_2 = (a_1 - a_2 + a_3 - a_4)(a_1 + a_2 + a_3 - a_4),\\
B &= B_1B_2 = (a_1 + a_2 - a_3 - a_4)(a_1 - a_2 - a_3 - a_4),\\
C &= C_1C_2 = (a_1 - a_2 - a_3 + a_4)(a_1 + a_2 - a_3 + a_4),\\
D &= D_1D_2 = (a_1 + a_2 + a_3 + a_4)(a_1 - a_2 + a_3 + a_4),\\
v_1 &= \tan\frac{\theta_1}{2},\ v_4 = \tan\frac{\theta_4}{2}.
\end{aligned}$$

The coefficients A, B, C, and D all split into a pair of bilinear factors each, A_1, A_2, B_1, etc.. In what follows, it is essential to maintain the definitions of the bilinear factors in Equation (6).

One of the advantages of this IO equation formulation is that the five remaining algebraic IO equations relating the five remaining distinct angle parameter pairings contain coefficients comprised of pairs of the same bilinear factors, but in different distinct permutations:

$$A_1B_2v_1^2v_2^2 + A_2B_1v_1^2 + C_1D_2v_2^2 - 8a_2a_4v_1v_2 + C_2D_1 = 0; \tag{7}$$

$$A_1B_1v_1^2v_3^2 + A_2B_2v_1^2 + C_2D_2v_3^2 + C_1D_1 = 0; \tag{8}$$

$$A_1D_2v_2^2v_3^2 + B_2C_1v_2^2 + B_1C_2v_3^2 - 8a_1a_3v_2v_3 + A_2D_1 = 0; \tag{9}$$

$$A_1C_1v_2^2v_4^2 + B_2D_2v_2^2 + A_2C_2v_4^2 + B_1D_1 = 0; \tag{10}$$

$$A_1C_2v_3^2v_4^2 + B_1D_2v_3^2 + A_2C_1v_4^2 + 8a_2a_4v_3v_4 + B_2D_1 = 0. \tag{11}$$

This is only possible using the DH relative joint angles, and not possible using the absolute joint angles, referenced to the positive x-axis of a non-moving coordinate system, as in the derivation of the Freudenstein equation [14, 15]. The parametric coupler point curve equation will be derived using Equation (7), the v_1-v_2 IO equation.

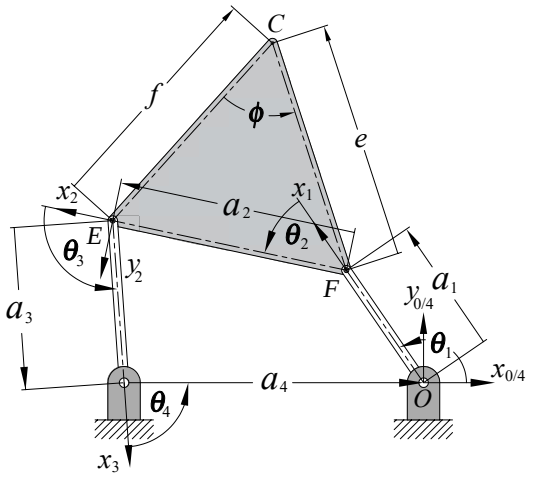

Fig. 2: Coupler curve generator parameters.

2 Trigonometric Coupler Point Curve Equation

One of the earliest recorded examples of mathematical methods of mechanical system design for guiding a point along a curve belongs to Archimedes [16], who lived ca. 287-212 BC. However, the very first patent [17] for a mechanism designed to move a point along a desired curve belongs to James Watt (1736-1819),

awarded more than 2000 years after Archimedes death. In the context of this paper, the coupler point curve is the locus of a point on a rigid body connected to two others moving on fixed centred circles in the plane. It is well known that the curve is a tricircular sextic having, at most, three real double points and three pairs of complex-conjugate intersections with the absolute circle in the plane, known as circular points [18, 19]. The first known work applied towards obtaining a trigonometric sextic equation describing the locus of the coupler point was published in 1875 by Samuel Roberts [1]. In his derivation, Roberts used the typical coordinate frame assignment whereby the non-moving coordinate system origin is at the centre of the left-most ground-fixed revolute joint with the positive x-axis pointing towards the centre of the right-most ground-fixed revolute joint and clockwise joint axis circulation.

It is a straightforward exercise to re-derive the trigonometric form of the coupler curve using the DH assignment convention and a counter clockwise joint axis circulation together with the geometric parameters illustrated in Figure 2. The slightly modified Roberts approach leads to the coupler curve equation in terms of the coupler point $C(x_0, y_0)$ in the non-moving ground-fixed coordinate system

$$(Q_1R_2 - Q_1R_1)^2 + (P_2R_1 - P_1R_2)^2 - (P_1Q_2 + P_2Q_1)^2 = 0, \tag{12}$$

where

$$\begin{array}{l|l} P_1 = -2ex_0, & P_2 = -2f\left(y_0\cos\phi + (a_4 - x_0)\sin\phi\right), \\ Q_1 = -2ey_0, & Q_2 = 2f\left((a_4 - x_0)\cos\phi - y_0\sin\phi\right), \\ R_1 = x_0^2 + y_0^2 + e^2 - a_1^2, & R_2 = x_0^2 + y_0^2 + f^2 + a_4^2 - 2x_0a_4 - a_3^2. \end{array}$$

This trigonometric implicit form of the coupler point curve equation has been used since its introduction in 1875 for examining the nature of the curve and its singular points because it does not depend on any variable joint angles.

3 Algebraic Coupler Point Curve Equation

For coupler curve synthesis and analysis problems where knowledge of the relationship between the mechanism configuration and the coupler point curve is needed, it can be argued that a more useful form of the coupler point curve equation for $C(x_0, y_0)$ is one in terms of the input angle $\theta_1 = 2\tan^{-1}(v_1)$. This is because the functional relationship between a point on the curve and the corresponding configuration of the linkage can be explicitly defined by the parametric equation. One way of determining this equation is to start with the v_1-v_2 IO equation. First, solve the equation for v_2, yielding two solutions, one for each assembly mode

$$v_2 = 4a_2a_4v_1 \pm \frac{\sqrt{-A_1A_2B_1B_2v_1^4 - A_1B_2C_2D_1v_1^2 - A_2B_1C_1D_2v_1^2 + 16a_2^2a_4^2v_1^2 - C_1C_2D_1D_2}}{A_1B_2v_1^2 + C_1D_2} \tag{13}$$

The next step is to compute the forward kinematics of the open 2R kinematic chain of the first two links, a_1 and a_2. The original DH coordinate system assignments and parameter convention [2] are used to describe the kinematic geometry of the open 2R chain, see Table 1 and Figure 3. Note that the link offset distances d_i and twist angles τ_i are not defined for planar linkages, and have only been included in Table 1 for completeness. The resulting forward kinematics coordinate

Axis	Angle v_i	Offset d_i	Length a_i	Twist τ_i
1	v_1	0	a_1	0
2	v_2	0	a_2	0

Table 1: DH parameters.

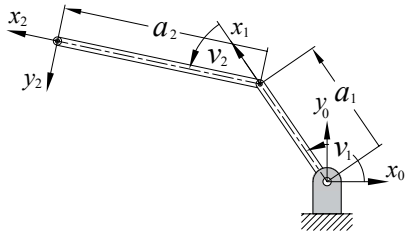

Fig. 3: Open 2R chain.

system transformation that maps point coordinates described in the coordinate system that moves with the coupler, $x_2,\ y_2$, to the non-moving ground-fixed coordinate system, $x_0,\ y_0$, in terms of the 4×4 homogeneous transformation matrix ${}^0\mathbf{T}_2$ is computed to be

$$ {}^0\mathbf{T}_2 \ = \ \begin{bmatrix} 1 & 0 & 0 & 0 \\ T_{21} & T_{22} & T_{23} & 0 \\ T_{31} & T_{32} & T_{33} & 0 \\ 0 & 0 & 0 & 1 \end{bmatrix}, \tag{14} $$

where

$$ T_{21} = \frac{((a_2 - a_1)v_2^2 - a_1 - a_2)v_1^2 - (4v_1)v_2 a_2 + (a_1 - a_2)v_2^2 + a_1 + a_2}{(v_1^2 + 1)(v_2^2 + 1)}, $$

$$ T_{22} = \frac{(v_2^2 - 1)v_1^2 - (4v_1)v_2 - v_2^2 + 1}{(v_1^2 + 1)(v_2^2 + 1)}, $$

$$ T_{23} = 2\left(\frac{(v_2 + v_1)(v_1 v_2 - 1)}{(v_1^2 + 1)(v_2^2 + 1)}\right), $$

$$ T_{31} = 2\left(\frac{((a_1 - a_2)v_2^2 + a_1 + a_2)v_1 + v_2 a_2 - a_2 v_1^2 v_2}{(v_1^2 + 1)(v_2^2 + 1)}\right), $$

$$ T_{32} = 2\left(\frac{(v_2 + v_1)(v_1 v_2 - 1)}{(v_1^2 + 1)(v_2^2 + 1)}\right), $$

$$ T_{33} = \frac{(v_2^2 - 1)v_1^2 - (4v_1)v_2 - v_2^2 + 1}{(v_1^2 + 1)(v_2^2 + 1)}. $$

This homogeneous transformation matrix requires the coupler point coordinates of point C described in the coupler coordinate system for a planar 4R mechanism to be defined in the following way:

$$C(x_2, y_2) = \begin{bmatrix} 1 \\ x_2 \\ y_2 \\ z_2 \end{bmatrix} = \begin{bmatrix} 1 \\ x_2 \\ y_2 \\ 0 \end{bmatrix} \tag{15}$$

The reason the three-dimensional homogeneous coordinates are used for the planar mechanism is for the generalisation of the planar mechanisms considered in this paper to the spherical and spatial mechanisms for future investigations.

Defining the coupler point coordinates in the coupler coordinate system that moves with the coupler, x_2, y_2, in this paper, requires a few words of discussion. Depending on the link lengths and coupler point, it will have different coordinates in each assembly mode when the coupler is mirrored. Consider the two assembly modes of the mechanism illustrated in Figure 4, with the coupler mirrored in the centre-line of a_2. The link lengths and coupler edge lengths are listed in Table 2. The coupler is an equilateral triangle and therefore possesses a coupler angle of $\phi = 60°$. For both the upper and lower assembly modes the coupler point in the coupler coordinate system has coordinates $C(x_2, y_2)_{U,L}$

$$C(x_2, y_2)_{U,L} = \begin{bmatrix} 1 \\ x_2 \\ y_2 \\ z_2 \end{bmatrix} = \begin{bmatrix} 1 \\ -\frac{5}{2} \\ -5\sin 60° \\ 0 \end{bmatrix}, \tag{16}$$

while the coordinates in the lower assembly mode with the mirrored coupler, $C(x_2, y_2)_{LM}$, are

$$C(x_2, y_2)_{LM} = \begin{bmatrix} 1 \\ x_2 \\ y_2 \\ z_2 \end{bmatrix} = \begin{bmatrix} 1 \\ -\frac{5}{2} \\ 5\sin 60° \\ 0 \end{bmatrix}. \tag{17}$$

Table 2: Link lengths and coupler edge lengths.

a_1	a_2	e	f	a_3	a_4
1	5	5	5	6	9

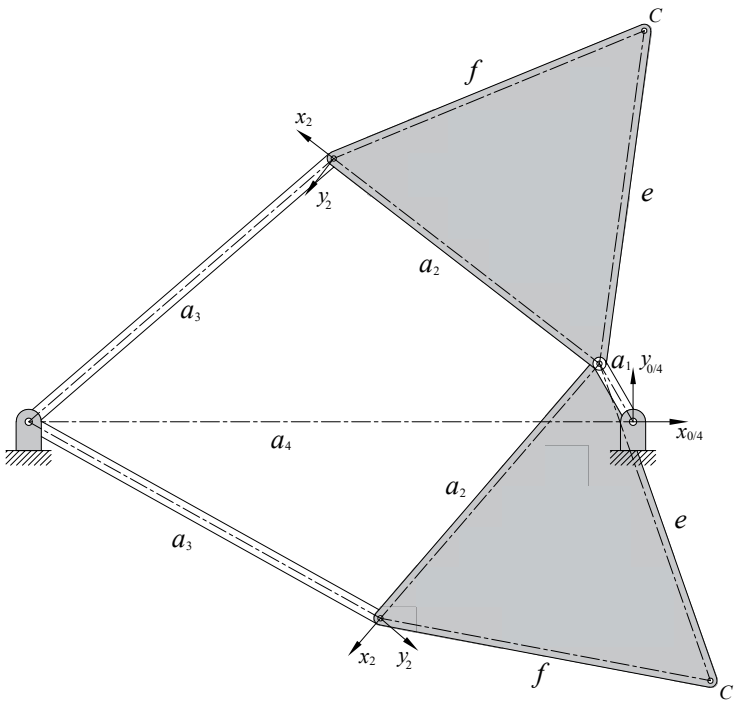

Fig. 4: Two assembly modes of a planar 4R with a mirrored coupler.

The next step is to determine the corresponding coupler point coordinates in the non-moving coordinate system $C(x_0, y_0)$ as

$$\begin{bmatrix} 1 \\ x_0 \\ y_0 \\ z_0 \end{bmatrix} = {}^0\mathbf{T}_2 \begin{bmatrix} 1 \\ x_2 \\ y_2 \\ z_2 \end{bmatrix}, \tag{18}$$

where $z_0 = z_2 = 0$. The final step in determining the coupler point curve in terms of the input joint angle parameter is to substitute Equation (13) into Equation (18) thereby eliminating v_2, which must be done for each assembly mode.

4 Example

In this example the parametric coupler point curve equation in both assembly modes, as well as in the lower assembly mode with the coupler mirrored in the centre-line a_2, will be determined for the mechanism illustrated in Figure 4 with link and coupler edge lengths listed in Table 2, and with coupler point coordinates

specified in Equations (16) and (17). The transformation ${}^0\mathbf{T}_2$, which is a function of only the v_1 angle parameter, is multiplied by the coupler point coordinates in the coordinate system that moves with the coupler, and the parametric equation of the coupler point curve in the non-moving coordinate system is obtained. The upper assembly mode parametric coupler point equation is

$$\begin{bmatrix} 1 \\ x_{0_U} \\ y_{0_U} \\ z_{0_U} \end{bmatrix}, \tag{19}$$

where

$$x_{0_U} = \frac{9177v_1^4 - 366v_1\sqrt{3}\sqrt{133v_1^4 + 258v_1^2 + 77} + 12024v_1^2 + 759}{-2128v_1^4 + 108v_1\sqrt{3}\sqrt{133v_1^4 + 258v_1^2 + 77} - 3644v_1^2 - 220} - \tag{20}$$

$$\frac{(258v_1^3 + 474v_1)\sqrt{3}\sqrt{133v_1^4 + 258v_1^2 + 77} - 7049v_1^6 - 19685v_1^4 - 16207v_1^2 - 979}{8(v_1^2 + 1)(532v_1^4 - 27v_1\sqrt{3}\sqrt{133v_1^4 + 258v_1^2 + 77} + 911v_1^2 + 55)} +$$

$$\frac{(3\sqrt{3}\sqrt{133v_1^4 + 258v_1^2 + 77} - 133v_1^3 - 169v_1)(3v_1\sqrt{3}\sqrt{133v_1^4 + 258v_1^2 + 77} - 47v_1^2 - 11)\sqrt{3}}{8(v_1^2 + 1)(-532v_1^4 + 27v_1\sqrt{3}\sqrt{133v_1^4 + 258v_1^2 + 77} - 911v_1^2 - 55)},$$

$$y_{0_U} = \frac{(399v - 1^2 + 33)\sqrt{3}\sqrt{133v_1^4 + 258v_1^2 + 77} - 5586v_1^3 - 3498v_1}{2128v_1^4 - 108v_1\sqrt{3}\sqrt{133v_1^4 + 258v_1^2 + 77} + 3644v_1^2 + 220} - \tag{21}$$

$$\frac{(3\sqrt{3}\sqrt{133v_1^4 + 258v_1^2 + 77} - 133v_1^3 - 169v_1)(3v_1\sqrt{3}\sqrt{133v_1^4 + 258v_1^2 + 77} - 47v_1^2 - 11)}{8(v_1^2 + 1)(-532v_1^4 + 27v_1\sqrt{3}\sqrt{133v_1^4 + 258v_1^2 + 77} - 911v_1^2 - 55)} -$$

$$\frac{((258v_1^3 + 474v_1)\sqrt{3}\sqrt{133v_1^4 + 258v_1^2 + 77} - 7049v_1^6 - 19685v_1^4 - 16207v_1^2 - 979)\sqrt{3}}{8(v_1^2 + 1)(532v_1^4 - 27v_1\sqrt{3}\sqrt{133v_1^4 + 258v_1^2 + 77} + 911v_1^2 + 55)},$$

and

$$z_{0_U} = 0. \tag{22}$$

The lower assembly mode parametric coupler point equation is

$$\begin{bmatrix} 1 \\ x_{0_L} \\ y_{0_L} \\ z_{0_L} \end{bmatrix}, \tag{23}$$

where

$$x_{0_L} = \frac{9177v_1^4 - 366v_1\sqrt{3}\sqrt{133v_1^4 + 258v_1^2 + 77} + 12024v_1^2 - 759}{-2128v_1^4 + 108v_1\sqrt{3}\sqrt{133v_1^4 + 258v_1^2 + 77} - 3644v_1^2 + 220} - \tag{24}$$

$$\frac{(258v_1^3 + 474v_1)\sqrt{3}\sqrt{133v_1^4 + 258v_1^2 + 77} - 7049v_1^6 - 19685v_1^4 - 16207v_1^2 - 979}{20(v_1^2 + 1)(532v_1^4 - 27v_1\sqrt{3}\sqrt{133v_1^4 + 258v_1^2 + 77} + 911v_1^2 + 55)} +$$

$$-\frac{(133v_1^3 + 3\sqrt{3}\sqrt{133v_1^4 + 258v_1^2 + 77} + 169v_1)(3v_1\sqrt{3}\sqrt{133v_1^4 + 258v_1^2 + 77} + 47v_1^2 + 11)\sqrt{3}}{20(v_1^2 + 1)(-532v_1^4 + 27v_1\sqrt{3}\sqrt{133v_1^4 + 258v_1^2 + 77} - 911v_1^2 - 55)},$$

$$y_{0_L} = \frac{(399v_1^2 + 33)\sqrt{3}\sqrt{133v_1^4 + 258v_1^2 + 77} - 5586v_1^3 - 3498v_1}{2128v_1^4 - 108v_1\sqrt{3}\sqrt{133v_1^4 + 258v_1^2 + 77} + 3644v_1^2 + 220} + \tag{25}$$

$$\frac{(3v_1\sqrt{3}\sqrt{133v_1^4 + 258v_1^2 + 77} - 47v_1^2 - 11)(-133v_1^3 + (3\sqrt{133v_1^4 + 258v_1^2 + 77})\sqrt{3} - 169v_1)}{20(v_1^2 + 1)(-532v_1^4 + 27v_1\sqrt{3}\sqrt{133v_1^4 + 258v_1^2 + 77} - 911v_1^2 - 55)} +$$

$$\frac{(258v_1^3 + 474v_1)\sqrt{3}\sqrt{133v_1^4 + 258v_1^2 + 77} - 7049v_1^6 - 19685v_1^4 - 16207v_1^2 - 979}{20(v_1^2 + 1)(532v_1^4 - 27v_1\sqrt{3}\sqrt{133v_1^4 + 258v_1^2 + 77} + 911v_1^2 + 55)},$$

and

$$z_{0_L} = 0. \tag{26}$$

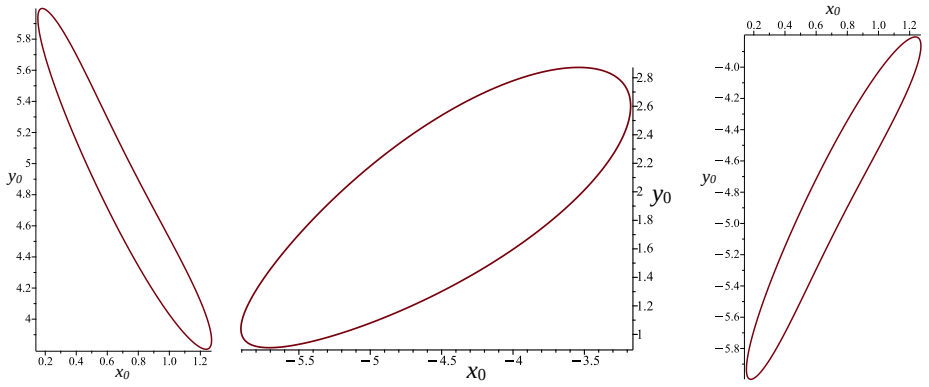

(a) Upper assembly mode.

(b) Lower assembly mode.

(c) Mirrored coupler.

Fig. 5: Coupler curves generated by the v_1-v_2 equation.

Finally, the parametric coupler point curve of the mirrored coupler in the lower assembly mode has the parametric equation

$$\begin{bmatrix} 1 \\ x_{0_{LM}} \\ y_{0_{LM}} \\ z_{0_{LM}} \end{bmatrix}, \tag{27}$$

where

$$x_{0_{LM}} = \frac{-9177v_1^4 - 366v_1\sqrt{3}\sqrt{133v_1^4 + 258v_1^2 + 77} - 12024v_1^2 - 759}{2128v_1^4 + 108v_1\sqrt{3}\sqrt{133v_1^4 + 258v_1^2 + 77} + 3644v_1^2 + 220} - \tag{28}$$

$$\frac{(-258v_1^3 - 474v_1)\sqrt{3}\sqrt{133v_1^4 + 258v_1^2 + 77} - 7049v_1^6 - 19685v_1^4 - 16207v_1^2 - 979}{8(v_1^2 + 1)(532v_1^4 + 27v_1\sqrt{3}\sqrt{133_v1^4 + 258v_1^2 + 77} + 911v_1^2 + 55)} +$$

$$\frac{(133v_1^3 + 3\sqrt{3}\sqrt{133v_1^4 + 258v_1^2 + 77} + 169v_1)(3v_1\sqrt{3}\sqrt{133v_1^4 + 258v_1^2 + 77} + 47v_1^2 + 11)\sqrt{3}}{8(v_1^2 + 1)(532v_1^4 + 27v_1\sqrt{3}\sqrt{133_v1^4 + 258v_1^2 + 77} + 911v_1^2 + 55},$$

$$y_{0_{LM}} = \frac{(-399v_1^2 - 33)\sqrt{3}\sqrt{133v_1^4 + 258v_1^2 + 77} - 5586v_1^3 - 3498v_1}{2128v_1^4 + 108v_1\sqrt{3}\sqrt{133v_1^4 + 258v_1^2 + 77} + 3644v_1^2 + 220} + \tag{29}$$

$$\frac{(133v_1^3 + 3\sqrt{3}\sqrt{133v_1^4 + 258v_1^2 + 77} + 169v_1)(3v_1\sqrt{3}\sqrt{133v_1^4 + 258v_1^2 + 77} + 47v_1^2 + 11)}{8(v_1^2 + 1)(532v_1^4 + 27v_1\sqrt{3}\sqrt{133_v1^4 + 258v_1^2 + 77} + 911v_1^2 + 55)} +$$

$$\frac{((-258v_1^3 - 474v_1)\sqrt{3}\sqrt{133v_1^4 + 258v_1^2 + 77} - 7049v_1^6 - 19685v_1^4 - 16207v_1^2 - 979)\sqrt{3}}{8(v_1^2 + 1)(532v_1^4 + 27v_1\sqrt{3}\sqrt{133_v1^4 + 258v_1^2 + 77} + 911v_1^2 + 55)},$$

and

$$z_{0_{LM}} = 0. \tag{30}$$

Figure 5 illustrates the coupler curves generated by the v_1-v_2 equation in each of the upper and lower assembly modes. As a graphical confirmation that the coupler point curve parametric equation is correct, Figure 6 illustrates the coupler curves as the locus of points of the selected coupler point generated independently by the software GeoGebra. It is easy to see that the coupler curves generated by the v_1-v_2 equation and by GeoGebra are congruent. Moreover the mirrored lower assembly mode coupler curve is the upper assembly mode coupler curve mirrored in the a_4 centre-line.

5 Conclusions

The algebraic IO equations for planar, spherical, and spatial 4R mechanisms have been investigated by the authors over the last seven years. The focus of

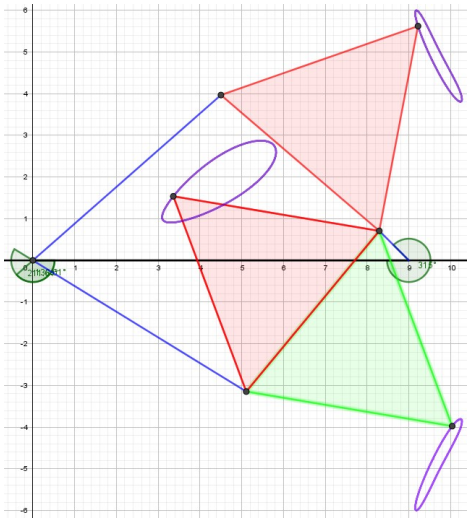

Fig. 6: Coupler curves generated in GeoGebra.

previous publications was on deriving the equations themselves and their time derivatives, examining the design parameter spaces, as well as continuous approximate kinematic synthesis for function generation between the six different IO pairs. In this paper, we have added to the new kinematic synthesis tools with a 4R planar coupler point curve analysis tool based on the v_1-v_2 IO equation and the forward kinematics transformation matrix of the open 2R a_1-a_2 kinematic chain leading to a parametric algebraic coupler point curve equation that is a function of the input angle parameter, v_1. The advantage of this formulation is that only one homogeneous transformation matrix needs to be computed, then it can be used to pre-multiply any coupler point. An example was presented for both assembly modes of arbitrary 4R planar mechanisms as well as the mirrored coupler in the lower assembly mode. The parametric coupler point curves are confirmed with an independent point locus computation using GeoGebra whereby congruent curves in each assembly mode are generated. It is also to be observed that the coupler point curve generated by the mirrored coupler in the lower assembly mode is the mirror of the coupler point curve in the upper assembly mode, reflected in the a_4 centre-line.

References

1. Roberts, S. "On Three-bar Motion in Plane Space." *Proceedings of The London Mathematical Society*, Vol. 7, p. 14–23, 1875.
2. Denavit, J. and Hartenberg, R.S. "A Kinematic Notation for Lower-pair Mechanisms Based on Matrices." *Trans ASME J. Appl. Mech.*, Vol. 23, p. 215–221, 1955.

3. Hartenberg, R.S. and Denavit, J. *Kinematic Synthesis of Linkages.* McGraw-Hill, Book Co., New York, N.Y., U.S.A., 1964.
4. Study, E. *Geometrie der Dynamen.* Teubner Verlag, Leipzig, Germany, 1903.
5. Selig, J.M. *Geometric Fundamentals of Robotics.* Springer Science + Business Media Inc, New York, NY, U.S.A., 2005.
6. Selig, J.M. "On the Geometry of the Homogeneous Representation for the Group of Proper Rigid-body Displacements." *Rom. J. Techn. Sci. – Appl. Mechanics*, Vol. 58, No. 1-2, pp. 153–176, 2013.
7. Pfurner, M. "The Family of Two Generator 3-Space Rulings of the Study Quadric." Private Communication, August 25, 2022.
8. Husty, M.L. and Schröcker, H.P. "Kinematics and Algebraic Geometry." In J.M. McCarthy, ed., "21st Century Kinematics," pp. 85–123. Springer-Verlag, London. doi:10.1007/978-1-4471-4510-3_4, 2013.
9. Hayes, M.J.D., Rotzoll, M., Bucciol, Q. and Copeland, Z.A. "Planar and Spherical Four-bar Linkage v_i–v_j Algebraic Input-output Equations." *Mechanism and Machine Theory*, Vol. 182, April 2023.
10. Rotzoll, M., Hayes, M.J.D., Husty, M.L. and Pfurner, M. "A General Method for Determining Algebraic Input-output Equations for Planar and Spherical 4R Linkages." In J. Lenarčič and B. Siciliano, eds., "Advances in Robot Kinematics 2020," pp. 90–97. Springer International Publishing, Cham, Switzerland, 2020.
11. Rotzoll, M. and Hayes, M.J.D. "A General Method for Determining Algebraic Input-output Equations for the Slider-crank and the Bennett Linkage." *11th CCToMM Symposium on Mechanisms, Machines, and Mechatronics*, Ontario Tech University, Oshawa, ON, Canada, 2021.
12. Rotzoll, M. *Algebraic Input-output Equations of Four-bar Kinematic Chains: Planar; Spherical; Spatial.* Ph.D. thesis, Carleton University, Ottawa, ON, Canada, 2023.
13. Husty, M.L. and Walter, D.R. "Mechanism constraints and singularities — the algebraic formulation." Vol. 589, pp. 101–180. Singular Configurations of Mechanisms and Manipulators, eds. A. Müller, D. Zlatanov, CISM International Centre for Mechanical Sciences, 2019.
14. Freudenstein, F. "An Analytical Approach to the Design of Four-link Mechanisms." *Trans. ASME*, Vol. 77, pp. 483–492, 1954.
15. Freudenstein, F. *Design of Four-link Mechanisms.* Ph.D. thesis, Columbia University, New York, N.Y., USA, 1954.
16. Ceccarelli, M. *Distinguished Figures in Mechanism and Machine Science, Their Contributions and Legacies Part 1.* Springer, New York, U.S.A., 2007.
17. Watt, J. "Patent No. 1432, April 28, 1784.", 1784.
18. Hilbert, D. and Cohn-Vossen, S. *Geometry and The Imagination,* English translation of *Anschauliche Geometrie*, 1932, by P. Nemenyi. Chelsea Publishing Company, New York, N.Y., U.S.A., 1952.
19. Hunt, K.H. *Kinematic Geometry of Mechanisms.* Clarendon Press, Oxford, England, 1978.